View metadata, citation and similar papers at core.ac.uk
brought to you by CORE
provided by Elsevier - Publisher Connector

Cell PRESS
Chemistry & Biology
Article

A PEF/Y Substrate Recognition and Signature Motif Plays a Critical Role in DAPK-Related Kinase Activity

Koen Temmerman,[1,2,4] Iñaki de Diego,[1,3,4] Vivian Pogenberg,[1] Bertrand Simon,[1] Weronika Jonko,[1] Xun Li,[1,2] and Matthias Wilmanns[1,*]
[1]European Molecular Biology Laboratory Hamburg, Notkestrasse 85, 22603 Hamburg, Germany
[2]European Molecular Biology Laboratory Heidelberg, Meyerhofstrasse 1, 69117 Heidelberg, Germany
[3]Present address: Molecular Biology Institute of Barcelona-Spanish National Research Council (IBMB-CSIC), c/Baldiri Reixac, 15-21, 08028 Barcelona, Spain
[4]These authors contributed equally to this work
*Correspondence: wilmanns@embl-hamburg.de
http://dx.doi.org/10.1016/j.chembiol.2013.12.008

SUMMARY

Knowledge about protein kinase substrate preferences is biased toward residues immediately adjacent to the site of phosphorylation. By a combined structural, biochemical, and cellular approach, we have discovered an unexpected substrate recognition element with the consensus sequence PEF/Y in the tumor suppressor death-associated protein kinase 1. This motif can be effectively blocked by a specific pseudosubstrate-type interaction with an autoregulatory domain of this kinase. In this arrangement, the central PEF/Y glutamate interacts with a conserved arginine distant to the phosphorylation site in sequence and structure. We also demonstrate that the element is crucial for kinase activity regulation and substrate recognition. The PEF/Y motif distinguishes close death-associated protein kinase relatives from canonical calcium/calmodulin-dependent protein kinases. Insight into this signature and mode of action offers new opportunities to identify specific small molecule inhibitors in PEF/Y-containing protein kinases.

INTRODUCTION

The human kinome comprises more than 500 members, and their abundance requires elaborate molecular mechanisms to regulate their catalytic activity and to generate substrate specificity (Pellicena and Kuriyan, 2006; Ubersax and Ferrell, 2007). About half of the serine/threonine (Ser/Thr) kinases utilize an arginine or lysine located amino-terminally of the phosphorylated residue as primary specificity determinant (Ben-Shimon and Niv, 2011; Zhu et al., 2005). Our knowledge of specificity-determining factors in protein substrates is mostly focused on the two to three residue positions next to their phosphorylation site (P0). For most kinases, positional information beyond these initial residues becomes ambiguous, yet several databases offer predictions beyond these limits (Ellis and Kobe, 2011; Hornbeck et al., 2012; Obenauer et al., 2003). However, synthetic peptide scanning libraries tend to be insensitive to flexible residues more remote from the central phosphorylation site (Alexander et al., 2011; Yaffe et al., 2001). Novel structures of kinase/substrate complexes could reveal interactions between the phosphorylation site and residues that may be distal in the substrate primary sequence but are in close proximity within the folded structure (Bialik and Kimchi, 2012).

A substantial fraction of all protein kinases have an autoregulatory domain (ARD) that is C terminal to the catalytic kinase domain (CD). The ARD can conditionally block the kinase active site by pseudosubstrate-type interactions until its removal by additional regulatory mechanisms such as calcium/calmodulin (Ca^{2+}/CaM) binding or site-specific phosphorylation (Kemp et al., 1994). A molecular analysis of these pseudosubstrate interactions would therefore provide new insights into the atomic details of kinase substrate specificity. To test such an approach, we have chosen death-associated protein kinase 1 (DAPK1) as a model of an ARD-containing protein kinase to unravel hitherto-unknown determinants of substrate specificity through a combined structural, biochemical, and functional approach. DAPK1 is an important tumor suppressor, is used as a diagnostic and prognostic tool during tumor development, and is a target for drug development (Raval et al., 2007; Schumacher et al., 2002). The protein contributes to development of the nervous system, yet the increased kinetic activity after neuronal injury or in neurodegenerative disease such as Alzheimer disease can be detrimental on neuronal protection (Fujita and Yamashita, 2013). The kinase domain of DAPK1 belongs to a branch of the kinome containing myosin light-chain-related kinases (MLCKs) and triple functional domain protein-related kinases, collectively referred to as DMT kinases (Temmerman et al., 2013).

Although previous positional scanning substrate library data have revealed moderate preferences for residues at positions next to the site of phosphorylation, an unambiguous substrate preference profile is still missing (Bialik et al., 2008; Lin et al., 2010; Velentza et al., 2001). Here, by direct structural comparison of different activity conformations of DAPK1, we discovered a specific interaction that is only found when the ARD of this kinase acts as pseudosubstrate. One of the binding partners

CrossMark

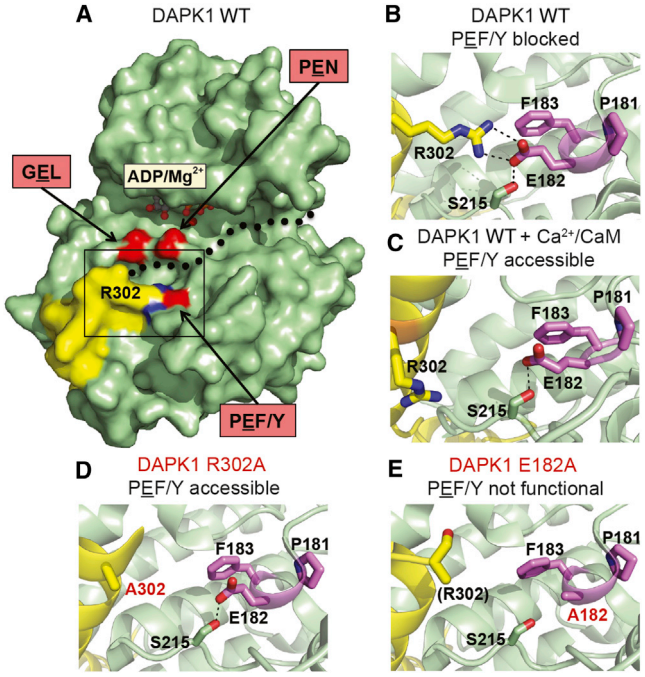

Figure 1. Conformation-Dependent Interaction of DAPK1 Glu182(CD, PEF/Y)-Arg302(ARD) as a Protein Kinase Activity Substrate Accessibility Determinant

(A) Surface representation of DAPK1 (apo conformation). Color codes: CD, light green; ARD, yellow. The approximate trace of the extended ARD pseudopeptide segment is indicated by a dotted line. The carboxylate groups of Glu100 (GEL motif), Glu143 (PEN motif), and Glu182 (PEF/Y motif) are highlighted in red. Glu182 is blocked by Arg302 (guanidinium group in blue) from the ARD and thus inaccessible for protein-substrate interactions.

(B–E) Close-ups of the boxed active site area show (B) apo-DAPK1 (WT) with Glu182 substrate inaccessible, (C) DAPK1-Ca^{2+}/CAM (WT) substrate accessible, (D) apo-DAPK1 (R302A) substrate accessible, and (E) apo-DAPK1 (E182A) nonfunctional; the R302 side chain is invisible and therefore marked between brackets. PEF/Y motif residues are labeled and colored in violet. Dashed lines indicate hydrogen bonds or salt bridges.

Complete structures used for this analysis are shown in Figure S1.

(Glu182) presents the central residue of the PEF/Y sequence motif that is highly conserved in a well-defined subset of the Ca^{2+}/CaM-dependent family of the human kinome. Functional in vitro and in vivo assays show that the removal of the side chain of Glu182 in the PEF/Y motif is sufficient to inhibit kinase activity. Likewise, we show that this motif can recognize distal (P-6) basic residues on the ARD pseudosubstrate (Arg302) as well as on peptide substrates.

RESULTS

Pseudosubstrate Interactions of the DAPK1 Autoregulatory Domain Are Conformation Dependent

As a starting point of our analysis, we used a recently determined DAPK1 structure in the presence of CaM, which revealed the complete ARD (residues 278–320) to be folded into a long α helix pointing away from the CD (de Diego et al., 2010). In this structure, CaM binds tightly to the ARD autophosphorylation site Ser308, thus sterically blocking this residue to become phosphorylated and indicating this conformation to be incompatible with that of a pseudosubstrate. To decipher a possible structural role for the DAPK1 ARD as a pseudosubstrate, we determined a complementary crystal structure of the same DAPK1 construct (residues 1–334, abbreviated as DAPK1 throughout this paper) in the presence of Mg^{2+}/ADP and in the absence of CaM (Figure 1A; Table 1; Figure S1 available online). In contrast to the structure of the DAPK1-CaM complex (de Diego et al., 2010), part of the ARD beyond the Ser308 phosphorylation site (residues 303–334) remained invisible, indicating a transient binding of Ser308 to the CD during autophosphorylation (Figure S2). In this structure, previously established protein substrate recognition motifs GEL (Glu100) and PEN (Glu143) (Zhu et al., 2005) are surface exposed and accessible. Figure S2 shows an overview of these motifs found in DAPK1.

Here, we focused on a comparison of ARD-CD interactions in the portion of the ARD visible in both DAPK1 structures, in the absence and presence of CaM (residues 278–302). The conformation of the N-terminal ARD part (residues 280–296), preceding the CaM-binding segment, is virtually identical in both structures; however, CaM binding induces significant alterations in the visible ARD-CD interactions in the subsequent segment (residues 297–302), most notably with Arg302 (Figures 1B and 1C). Whereas in the apo-DAPK1 structure Arg302 interacts via a direct salt bridge with the CD residue Glu182, next to the activation segment, in the DAPK1-CaM complex the same residue is reoriented and involved in CaM interactions (de Diego et al.,

Table 1. X-Ray Data Collection and Refinement Statistics

Protein name	DAPK1 WT	DAPK1 E182A	DAPK1 R302A
PDB entry	2W4K	2XUU	4B4L
X-ray data collection			
Space group	$P2_12_12_1$	$P2_12_12_1$	$P2_12_12_1$
Wavelength (Å)	0.976	0.873	0.873
Cell dimensions *a, b, c* (Å)	49.3, 77.0, 108.9	49.7, 84.4, 86.3	49.4, 83.8, 84.6
Resolution (Å)[a]	62.9-1.90 (2.00-1.90)	30.4-1.80 (1.90-1.80)	59.5–1.75 (1.84-1.75)
Completeness (%)[a]	97.8 (87.9)	100 (99.9)	100 (99.9)
R_{sym}[a]	0.072 (0.535)	0.110 (0.560)	0.123 (0.991)
Mean (I/sI)[a,b]	11.7 (2.7)	9.3 (2.5)	12.7 (2.1)
Redundancy[a]	3.7 (3.3)	4.0 (4.0)	6.7 (6.9)
Structure determination and refinement			
Resolution (Å)	62.9-1.90	30.4-1.80	59.5–1.75
No. reflections	30,930	34,469	34,315
R_{cryst}/R_{free}	0.195/0.228	0.179/0.226	0.193/0.220
No. atoms protein/ ions/ligands/solvent	2,463/1/27/ 271	2,411/16/27/ 408	2,428/35/48/ 266
B factors (Å^2) protein/ ligands/solvent	25.7/27.1/ 38.3	18.3/23.4/ 31.8	19.1/42.4/ 28.9
Rmsd bond lengths (Å)	0.012	0.026	0.020
Rmsd bond angles (°)	1.333	2.009	1.991

[a]Values in parentheses refer to highest-resolution shell.

[b]I/σI indicates the average of the intensity divided by its average SD. R_{free} is the same as R_{value} for the 5% of the data randomly omitted from refinement.

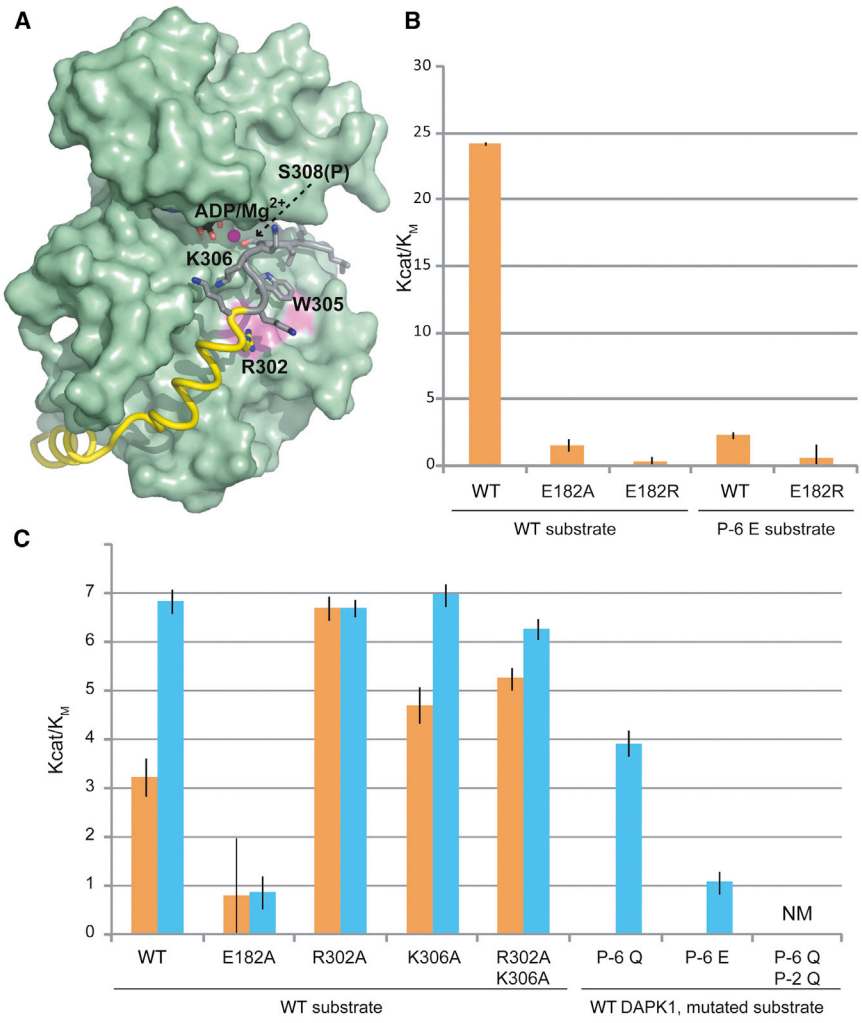

Figure 2. Opposite Functional Effects of DAPK1 Glu182 and Arg302 in Substrate Recognition and Autoinhibiton Release

(A) apo-DAPK1, extended with a model of ARD residues 303–311 (gray). The CD is shown by surface presentation and the ARD by ribbon presentation. Residues mutated for functional studies and relevant for autoinhibition or CaM binding are labeled. Color codes are as in Figure 1.

(B and C) Histogram of steady-state activity kinetics of DAPK1(CD) (B) or DAPK1 (C) variants using an MLC-2-derived peptide KKRPQRRYSNVF or variants in which either positions P-6 or P-2 (underlined), in reference to the phosphorylation site (in italics), or both have been altered (for further details, see Table S1). CaM absent, orange bars; CaM present, cyan bars. Values of k_{cat}/K_M (specificity constant) are indicated in ±SEM. NM signifies nonmeasurable; the corresponding activity cannot be correctly analyzed by Michaelis-Menten kinetics.

2010). To investigate whether the Glu182(CD)-Arg302(ARD) interaction is essential for the ARD conformation observed in the apo-DAPK1 structure, we also solved the structures of two DAPK1 mutants, E182A and R302A, in which one of two side chains required for salt-bridge formation was removed (Figures 1D and 1E; Figure S1). The two structures confirm that the N-terminal ARD helix is formed and oriented as in the wild-type (WT) DAPK1 structure, indicating that the Glu182-Arg302 interaction is not essential for maintaining any specific conformation of the active site. Indeed, irrespective of whether Glu182 is blocked by an interaction with Arg302 or surface exposed, its consistent orientation in all structures is supported by a flanking interaction with Ser215.

To ultimately understand the relation of the ARD pseudosubstrate to different substrate binding motifs and to guide designing further mutants in the pseudosubstrate segment of the ARD, we modeled residues 303–311 that are subsequent to the final visible residue in the apo-DAPK1 structure (Figure 2A; Figure S1). This model correctly positions Ser308 (P0) at the DAPK1 active site, in agreement with previous substrate peptide complexes of phosphorylase kinase and CaMKII (Chao et al., 2010; Lowe et al., 1997).

Based on the structural data of autoinhibited DAPK1, we reasoned that Arg302 could represent an important pseudosubstrate P-6 specificity site for Ser308 phosphorylation. Vice versa, our data suggest that Glu182 could be a key residue for recognizing the −6 position of the DAPK1 ARD or, when released from a pseudosubstrate conformation by CaM binding, for recognizing structurally equivalent positions in DAPK1 protein substrates that are remote (i.e., five or more residues) from the site of phosphorylation. These hypotheses predict that Glu182 removal should reduce or even abolish DAPK1 kinetic activity whereas removal of Arg302 could lead to an enhanced *trans*-phosphorylation activity by unblocking the Glu182 substrate recognition site.

The Residue Pair Glu182-Arg302 in DAPK1 Functions as a Substrate Recognition Module

To assess these potential functional roles, we measured the kinase activity of several DAPK1 variants through two complementary approaches: (1) an enzymatic in vitro assay, using a peptide derived from myosin regulatory light chain 12B (MLC-2) as a potent substrate (de Diego et al., 2010; Velentza et al., 2001); and (2) an in vivo cellular characterization of DAPK1 variants.

The DAPK1 E182A mutant showed only residual in vitro enzymatic activity regardless of the presence of CaM (Figure 2C; Table S1), indicating that this side chain is crucial for catalytic DAPK1 activity. Indeed, even the activity of the unregulated DAPK1(CD) E182A version, which lacks the ARD, was severely impaired (Figure 2B; Table S1). The charge-reversal mutant DAPK1(CD) E182R further reduced activity to a specificity constant (k_{cat}/K_M) of about 1% of WT DAPK1. Because the position of Glu182 suggests that it has no direct involvement in either

nucleotide turnover or phosphate transfer onto a protein substrate, the most plausible structure-based explanation is that its negatively charged side chain is essential for DAPK1 protein substrate recognition. This finding is supported by isothermal titration calorimetry (ITC) data showing that nucleotide binding, with a K_d of 1–2 μM, is not affected by mutating E182. Consequently, binding defects are confined to the DAPK1 peptide substrate (Figure S3).

We also tested the DAPK1 activity effect by exchanging the P-6 arginine in the MLC-2 peptide substrate (Figures 2B and 2C; Table S1) with a glutamine and glutamate, leading to effective charge reversal. The K_M and specificity constant of the P-6Q peptide variant were about half that of WT, with a further 4-fold reduction observed for the P-6E peptide. The unregulated DAPK1(CD) even displayed a drop in K_M toward the mM range and a 10-fold reduced specificity constant. This observation is remarkable considering the proximity to the N terminus of the peptide used, which probably has a more floppy conformation. A charge inversion setup, using the P-6E peptide and DAPK1(CD) E182R, was not able to restore the kinase activity. Possibly, the DAPK1 E182R mutant engages in other interactions within the kinase domain, rendering the residue inaccessible for substrate binding. When both P-6 and P-2 sites were mutated to glutamine, we did not find any phosphorylation of the respective MLC-2 peptide variant, demonstrating that the two sites combined are essential for MLC-2 substrate recognition by DAPK1. These data are analogous to previous results on MLC-2 phosphorylation by MLCK (Kemp et al., 1983). Interestingly, these studies also indicated that extending the distance between the physiological Ser19 phosphorylation site and the basic residues normally around P-6 shifted the phosphorylation presence to the neighboring Thr18 (Kemp and Pearson, 1985). Compared to the loss of catalytic activity in the E182A mutant, the opposite effect is seen when the interaction partner of Glu182 in the DAPK1 apo conformation, Arg302 from the ARD, is mutated. In the presence of CaM, DAPK1 activity is not affected. However, the R302A mutation considerably releases the activity inhibition in the absence of CaM, resulting in a k_{cat} equivalent to the level of CaM-bound WT DAPK1 (Figure 2C; Table S1). Our structural data suggest that in the absence of the Glu182-Arg302 salt bridge in apo-DAPK1, which is impaired in the DAPK1 R302A mutant, Glu182 becomes accessible as the substrate recognition site. For comparison, we also tested the effects of the ARD P-2 site Lys306, previously characterized as possible substrate recognition site in synthetic peptides (Velentza et al., 2001), and the two sites (Arg302 and Lys306) combined. The respective DAPK1 variants (K306A and R302A + K306A) show a similar effect on DAPK1 activity in the absence of CaM; however, the increase in k_{cat} of K306A alone is inferior compared to that found for R302A. This could be because of increasing flexibility of the ARD near the Ser308 phosphorylation site, thus leading to less effective masking by the ARD of additional previously characterized kinase substrate recognition sites (Zhu et al., 2005). The K_M values of the ARD mutants do not significantly differ from the WT enzyme, as the mutations do not affect the kinase domain itself. The increased catalytic constants k_{cat} appear to depend on the facilitated release of the ARD. The opposite is seen for the E182A mutation on the kinase domain, which strongly influences the K_M (Table S1).

Whereas the CaM-bound form of DAPK1 represents an active form of the protein, the opposite is achieved by S308 autophosphorylation, which inhibits CaM binding (Shohat et al., 2001). Indeed, a phospho-mimicking DAPK1 mutant S308D attenuated the activating effect of R302A (Table S1). The level of S308 autophosphorylation was not diminished in the DAPK1 ARD mutants investigated, indicating that increased flexibility at the N-terminal part of the DAPK1 ARD does not hinder positioning S308 into the DAPK1 active site (Figure S4A). Indeed, the increased level of autophosphorylation found in the DAPK1 R302A mutant may indicate an enhancement of correct positioning of S308 into the active site due to increased ARD flexibility, in the absence of the E182-R302 salt bridge observed in the WT DAPK1 structure (Figure 1). In agreement with our structural data, the DAPK1 mutants investigated do not have a significant effect on CaM binding (Figure S4B). To assess the extent of S308 autophosphorylation influence on kinetic experiments with added CaM, DAPK1 was coexpressed with CaM (Table S1), effectively shielding S308 for autophosphorylation. In agreement with the determined autophosphorylation levels, the specificity constant of DAPK1 WT is slightly increased and this effect is more pronounced for DAPK1 R302A.

For our cellular assay, the setup of the in vitro kinetic experiments was mimicked. First, we transfected human embryonic kidney 293 (HEK293) cells with WT and mutant DAPK1(CD) alone. Next, we applied WT and mutant DAPK1 without or with thapsigargin (TG) treatment to activate DAPK1 by CaM binding. Overexpressing the deregulated CD of DAPK1, without the ARD, confirmed a strong blebbing effect (Figures 3A and 3B). When we removed the Glu182 side chain in the CD fragment, blebbing was reduced 2-fold. As for the biochemical experiments, the DAPK1 charge-reversal mutation E182R led to a further 2-fold reduction in blebbing. This indicates that loss of this substrate recognition site has a significant effect on cellular MLC-2 phosphorylation. By contrast, regulated DAPK1 with the ARD attached did not show significant blebbing, in agreement with previous studies (Bialik et al., 2004; de Diego et al., 2010).

Next, we treated the cells with TG, which increases the intracellular Ca^{2+} concentration and, concordantly, active Ca^{2+}/CaM. This approach confirmed that WT ARD-containing DAPK1 could be activated by about 10-fold, whereas in E182A this effect was considerably reduced (Figures 3A and 3B). The influence of Arg302 and Lys306 on DAPK1 autoinhibition was similarly characterized in the cellular assay but without the TG treatment. Confirming the kinetic data in the absence of Ca^{2+}/CaM, the R302A mutation was sufficient to activate DAPK1 by about 2-fold (Figure 3C). By contrast, K306A alone did not alter the blebbing phenotype, nor was there a significant additive effect when this mutation was combined with R302A.

DISCUSSION

Preferred sequence patterns near the site of phosphorylation, generally up to two to three residues, have been systematically analyzed for various kinases by well-established profile scanning approaches (Ubersax and Ferrell, 2007; Yaffe et al., 2001). Based on these data, distinct substrate recognition sites have been classified into motifs and comprise a glutamate or aspartate embedded into highly conserved residues. Three such

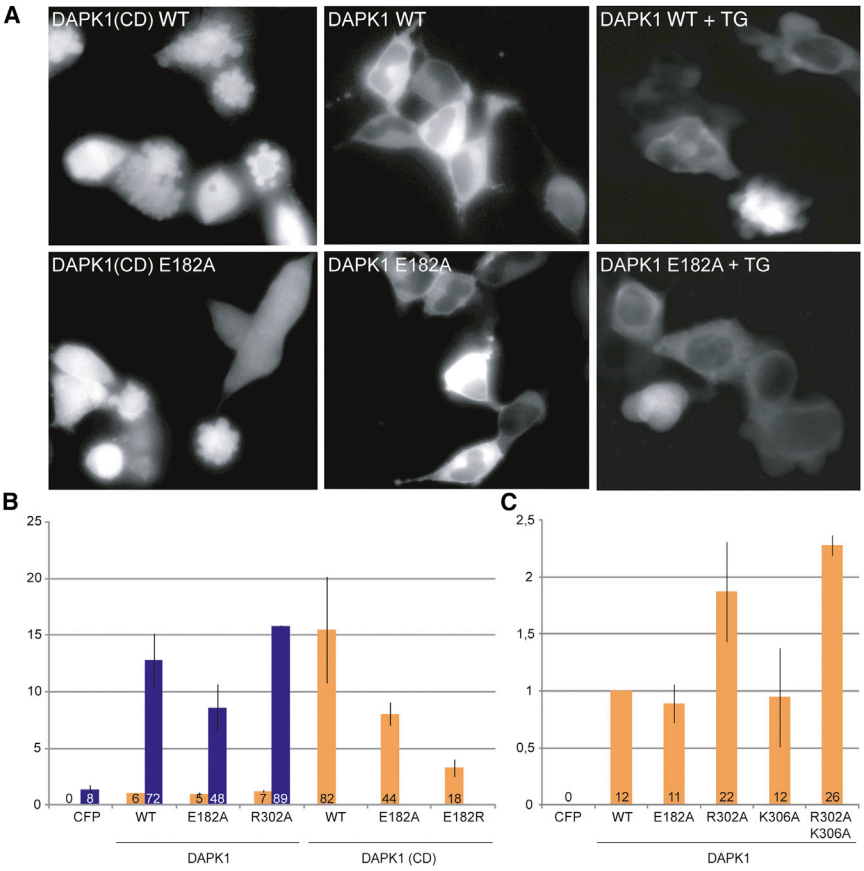

Figure 3. DAPK1 Glu182 Is Required for MLC-2-Dependent Membrane Blebbing in Cells

(A) Representative images of HEK293 cells expressing ECFP fusions of the indicated proteins. Overexpression of DAPK1 CD causes dynamic membrane blebbing (upper left panel), which is reduced by the introduction of E182A (lower left panel). Cells overexpressing WT or E182A DAPK1 display a normal morphology, unless treated with thapsigargin (TG), with the most pronounced blebs on WT cells (upper right panel).

(B and C) Relative amount of DAPK1 variant-expressing cells showing membrane blebbing 24 hr (B) or 48 hr (C) posttransfection. Orange bars, untreated cells; dark blue bars, cells with TG added; CFP was used as control. For (B) and (C), WT DAPK1 blebbing was normalized to 1; the average of at least two independent experiments ±SEM, each with n > 100, is depicted. The actual percentage of blebbing cells is indicated within the bar for each condition or variant.

motifs, which are surface exposed on loop segments near the kinase active site, have been described in detail (Figure S2). The final basic residue positional preference strongly depends on the juxtaposition of each of these motifs, yet reasonable predictions can be made (Ben-Shimon and Niv, 2011). The general motif GEL (residues 99–101 in DAPK1 and 127–129 in PKA C-α) confers specificity toward position P-3 (Fujii et al., 2004; Yaffe et al., 2001). This motif is found in most AGC kinases (including the representative members cAMP-dependent protein kinase 1 [PKA], cGMP-dependent protein kinase, and protein kinase C) as well as in CAMK family members. Two other motifs, PEN and YEM, have been found to provide a strong preference toward the P-2 site and, in some cases, toward the P-5 site (Yang et al., 2002), of which only the PEN can be found in CAMKs (142–144 in DAPK1 and 170–173 in PKA C-α). In addition, nonconserved acidic patches have been found that confer preference to basic residues on other sites, for example a DDD/E signature (D226–228 in AMPKα-1) for P-6 in the AMPK/BRSK branch of CAMKs (Scott et al., 2002).

In contrast, little is known about substrate conformational requirements, which may translate in specific sequence preferences more remote from the site of phosphorylation. In this study, we have identified and characterized a substrate recognition motif that we refer to as PEF/Y (residues 181–183 in DAPK1, 203–205 in PKA C-α) by direct comparison of DAPK1 structures in an autoinhibited conformation, in which the ARD functions as pseudosubstrate, and in the presence of Ca^{2+}/CaM, which leads to DAPK1 activation. The central residue of the PEF/Y, Glu182, recognizes the P-6 site (Arg302) of the DAPK1 ARD phosphorylation site (Ser308), and our structural data show that this site is in an α-helical conformation, establishing specific conformational restrictions in placing and orienting all residues that are located on the helical sequence segment.

In contrast to GEL and PEN, the PEF/Y motif is situated at the lower lobe of DAPK1, within a hairpin turn that defines the C terminus of the activation segment, and remote from the nucleotide-binding pocket (Figure 1A; Figure S2). Although the first two residues of the PEF/Y motif are invariant in all DAPK1-related protein kinase sequences, the third residue of the motif is either a phenylalanine or tyrosine (Figure 4). Our structural data indicate that role of the proline is restricting and thus defining a highly specific conformation and orientation of the PEF/Y-containing loop. The motif resides in the so-called P+1 loop due to its significance in accommodating the neighboring residue of the substrate phosphorylation site in many kinases (Goldsmith et al., 2007). PKA C-α residues L199, P203 (of the PEF/Y motif), and L206 form a hydrophobic pocket for P+1 (Figure S2). Immediately following L206 is the generally conserved APE motif (Figure 4), which firmly anchors this entire loop to the F helix at the core of the lower kinase lobe (Kornev and Taylor, 2010). Although phosphorylation is a prerequisite of the activation loop and consequent rearrangement in the P+1 loop/APE motif for PKA C-α as for most kinases (Steichen et al., 2010), this is not the case for DAPK. Instead, the activation loop is fixed by an alternative hydrophobic anchor unique to DMT kinases (Temmerman et al., 2013), rendering the PEF/Y and P+1 loop immobile.

Remarkably, there is a sharp distinction between DAPK1-related protein kinases (Temmerman et al., 2013) and canonical CaM-dependent protein kinases, such as CaM kinases I–IV, which lack the PEF/Y motif (Figure 4; Table 2). Several structures of the latter and peptide substrate complexes of CaMKII (Chao

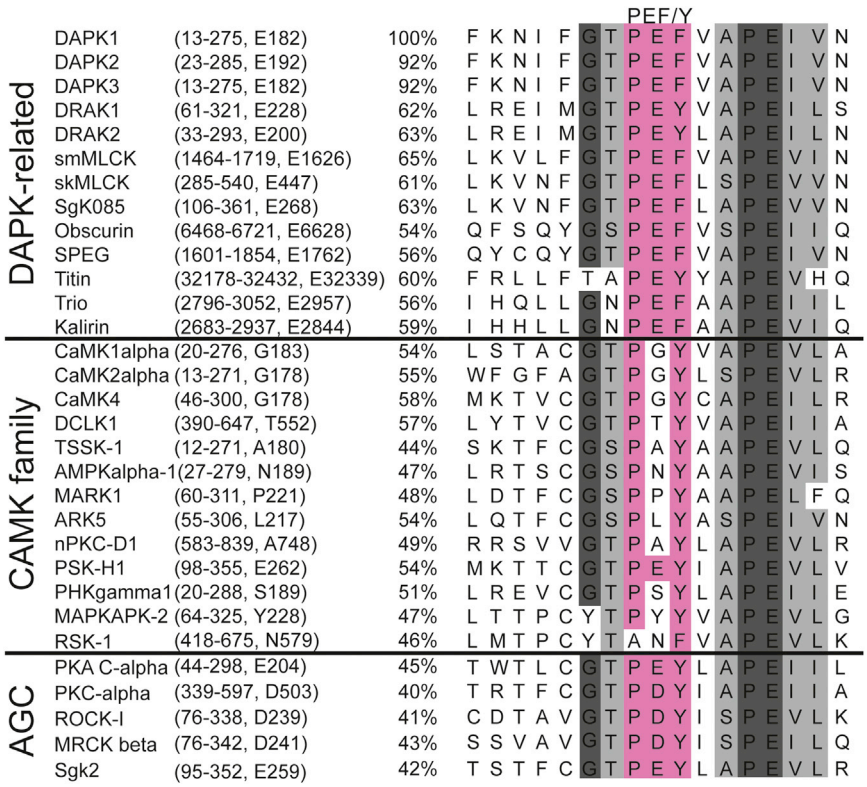

Figure 4. Multiple Sequence Alignment of the Residues Next to the PEF/Y Motif of Representative Kinases of the CAMK Family

Protein names, CD sequence range, position of the central PEF/Y residue, and the level of sequence similarity to DAPK1 (in %) are listed to the left. Conserved PEF/Y motif residues are colored in pink, and other conserved residues are in light gray (cluster of similar amino acids) or dark gray (invariant). DAPK1-related kinases that establish a separate branch in a phylogenetic tree of CAMK family kinases (Temmerman et al., 2013) have the PEF/Y motif in common, whereas this motif is missing in all canonical CaM kinases and almost all other related kinases. A representative selection of AGC kinases is given as reference.

et al., 2010) confirm there is no specific recognition of the equivalent site in DAPK1. The structures of the related CDs of DAPK2, DAPK3, DRAK2, titin, and MLCK corroborate that this side chain is spatially conserved within DAPK-related kinases. Moreover, DAPK2 possesses an ARD highly similar to DAPK1 (Temmerman et al., 2013) and is likely to follow the same regulation pattern as described here for DAPK1. By contrast, DAPK3 contains a C-terminal leucine zipper structure instead of an ARD (Kawai et al., 1998), which consequently differs in activation mode and undergoes autophosphorylation on nonconsensus sites (Pike et al., 2008). The most remarkable autophosphorylation for DAPK3 is on Thr180, immediately adjacent to the PEF/Y motif, which promotes activation. Indeed, a T180A mutation abolishes kinase activity (Graves et al., 2005). DAPKs are constitutively active and do not require phosphorylation to switch the active site on (Temmerman et al., 2013). Therefore, a DAPK3 T180 alteration could lead to a direct relocation of the PEF/Y motif and a subsequent effect on substrate affinity and kinase activity. In the case of titin, which comprises an ARD-containing kinase likely not regulated by CaM (Mayans et al., 2013; Temmerman et al., 2013), the central PEF/Y glutamate instead interacts with a tyrosine from the ARD N terminus (Mayans et al., 1998). This interaction renders the active site inaccessible for protein substrates and thus inactive. Interestingly, phosphorylation of Tyr170 next to the PEF/Y motif in titin kinase has been shown to activate this kinase, leading to a model in which loss of the ARD interaction by Glu169 would render the PEF/Y motif accessible as a substrate recognition site.

Next to the CAMK family, the PEF/Y motif is also present in the vast majority of AGC kinases (Figure 4; Table 2). However, any functional implications remain largely uninvestigated to date. The only known example has been a study on PKA that used a structure of this kinase in complex with a peptide substrate (Moore et al., 2003). In this structure, the peptide arginine at P-6 interacts with the central PEF/Y glutamate as well, reminiscent to our observations in DAPK1. As for the DAPK1 ARD, the PKA peptide substrate P-6 position is within an α-helical environment, which impacts the site's positioning within the kinase active site. Similar to DAPK1, mutation of the PEF/Y glutamate in PKA reduces catalytic activity. The expected general significance of the PEF/Y motif in other members of the human kinome is underlined by observations of at least three kinases, by screening specific cancer cell lines, for which mutations in this motif give rise to a pathological phenotype (Table 2).

A crucial question remains whether PEF/Y-mediated remote substrate recognition is a common property of all PEF/Y motif-comprising kinases (Table 2). Our data and previous structural studies on DAPK1 substrates (Lin et al., 2010) indicate that there is a conformational tolerance around the substrate residue at P-6, with some substrates forming loop regions and others helices (Figure 5). This may explain why there may be positional tolerance in the recognition of *trans*-phosphorylation substrates, rendering a sequence-based substrate recognition pattern less obvious. Ultimately, structural constraints in potential substrates could serve as an additional parameter beyond mere sequence constraints, thus introducing a new concept in deciphering substrate specificity in protein kinases. It would also be interesting to further investigate how our findings on the importance of the PEF/Y in regulating DAPK1 activity combines with other regulatory mechanisms such as additional sites for phosphorylation to generate potentially even more activated or inhibited conformational states of this and related kinases.

SIGNIFICANCE

Protein kinases have substantial variation in the protein substrate recognition sites, leading to highly specific

Table 2. Human Kinase Genes with a PEF/Y Motif

DAPK related	PEF	*DAPK1, DAPK2, DAPK3,* ***KALRN****, MYLK, MYLK2, MYLK3, MYLK4, OBSCN SPEG, TRIO*
	PEY	*DRAK1, DRAK2, TTN*
AGC family	PEF	*PKN1, PKN2, PKN3*
	PEY	*AKT1, AKT2, AKT3, DMPK*, DMPK2*, MAST1, MAST2, MAST3, MAST4, MRCKa*,* ***MRCKb****, PRKACA, PRKACB, PRKACG, PRKCA*, PRKCD*, PRKCD*, PRKCE*, PRKCG*, PRKCH*, PRKCQ*, PRKG1, PRKG2, PRKX, PRKY, SGK1,* ***SGK2,*** *SGK3, STK38*, STK38L*, ROCK1*, ROCK2**
Other	PEF	*Wnk1, Wnk2, Wnk3, Wnk4*
	PEY	*CAMKV, PSKH1, PSKH2, SCYL2*

Classification into groups according to the kinase family and type of motif (Manning et al., 2002). Genes for which cancer-related mutations have been identified within the PEF/Y motif are in bold (*SGK2* and E259K Greenman et al., 2007; *MRCKb* and D241H; Wang et al., 2007; *KALRN* and E2844G; Barretina et al., 2012). AGC family members containing an equivalent PDY variant of PEY are marked with an asterisk.

kinase/substrate relations. In general, kinases substrates are recognized linearly by specific residues next to the site of phosphorylation that bind to kinase-specific sequence motifs within or near the active site. However, increasing evidence is emerging that substrate sequence features more remote from the site of phosphorylation and their structural conformation may have crucial contributions to specific kinase/substrate relations as well. To address this point, we have used death-associated protein kinase as a model, as its mode of activity regulation is well established. Here, we have discovered a sequence motif (we refer to as PEF/Y) that recognizes the –6 position (Arg302) in an α-helical conformation of the C-terminal pseudosubstrate region of this kinase in its autoinhibited state. Our structural and complementary functional data indicate that this PEF/Y motif is crucial for the recognition of equivalent positions in other *trans*-substrates of this kinase as well. Because the PEF/Y motif is only found in specific groups of protein kinases, including those closely related to death-associated protein kinase, it has a capacity to serve as marker of protein kinase substrate specificity. Our data advance the understanding of the mechanistic basis of substrate recognition by kinases. Structure-based substrate recognition could provide a kinase-specific fingerprint, opening new leads on kinase inhibitors that do not target the active site. In the case of death-associated protein kinase, for which activity is linked to both tumor suppression and neuronal degradation, specific inhibitors for one pathway are highly desirable.

EXPERIMENTAL PROCEDURES

Cloning, Expression, and Purification

Homo sapiens DAPK1 (CD, residues 1–285) and DAPK1 (residues 1–334) were amplified by PCR from a full-length human *DAPK1* cDNA and cloned into pETM11 and pETM30 vectors, respectively. For cellular experiments, the same constructs were cloned into a pECFP-C1 vector (Clontech). Site-directed mutagenesis by PCR was used to generate DAPK mutant variants. Cells were grown in Luria broth (LB) media supplemented with 30 μg/ml kanamycin to an optical density 600 of 0.6–0.8. Protein expression was induced at 20°C for 16 hr in the presence of 200 μM isopropyl β-D-1-thiogalactopyranoside. For purification of the DAPK1 variants, cells were harvested and sonicated in 300 mM NaCl, 5% glycerol, 20 mM imidazole (pH 8), 8 mM 2-mercaptoethanol, and protease inhibitors buffered in 50 mM HEPES (pH 7.2). Cleared supernatants were filtered and applied to Ni-NTA beads (QIAGEN) and protein was eluted with 300 mM imidazole. For kinase activity assays, cells were harvested and sonicated in 150 mM NaCl, 5% (v/v) glycerol, 0.5 mM tris(2-carboxyethyl)phosphine (TCEP), 10 μg/ml lysozyme, and protease inhibitors buffered in 50 mM HEPES (pH 7.2); the protein was applied to Glutathione Sepharose 4B (GE Healthcare) and eluted with 10 mM glutathione. In all cases, protein was dialyzed overnight to 120 mM NaCl, 4mM $CaCl_2$, and 8 mM 2-mercaptoethanol (0.5 mM TCEP for kinetic assays), buffered in 30 mM HEPES (pH 7.2), in the presence of TEV protease at a 1:50 molar ratio for tag cleavage. The cleaved tag was removed and samples were further purified by size exclusion chromatography. Selected fractions were collected and concentrated to 10–17 mg/ml (for crystallization) or 1–1.6 mg/ml (for kinase activity assays). For crystallization purposes, 1 mM phenylmethanesulfonylfluoride (PMSF) was added to the final protein solution.

X-Ray Data Collection and Structure Determination

Crystals were obtained by the sitting drop vapor diffusion technique at the EMBL Hamburg Crystallization Facility. A total of 0.2–0.3 μl of protein were dissolved at 12–17 mg/ml in 30 mM HEPES (pH 7.2), 120 mM NaCl, 6 mM $CaCl_2$, 8 mM 2-mercaptoethanol, and 1 mM PMSF and mixed with an equal volume of reservoir buffer. Crystallization drops were equilibrated at 19°C against 80 μl of reservoir buffer, including 5 mM $MgCl_2$ and 5mM ADP, except for DAPK1(R302A). DAPK1(WT) crystals were obtained from 170 mM $(NH_4)_2SO_4$, 25% [w/v] PEG 4000, and 15% (v/v) glycerol. DAPK1(E182A) crystals were obtained from 200 mM Li_2SO_4, 25% (w/v) PEG 4000 buffered in 100 mM Bis-Tris (pH 5.5). DAPK1(R302A) crystals were obtained in 200 mM $(NH_4)_2SO_4$ and 25% (w/v) PEG 3350 buffered in 100 mM Bis-Tris (pH 5.5). Each crystal form was verified by MALDI-TOF (Applied Biosystems, Voyager) on protein completeness.

Crystals were shock frozen in mother liquor, and X-ray data were collected at 100 K. X-ray data sets were collected at beamlines BM14 (EMBL Grenoble/European Synchrotron Radiation Facility [ESRF]), ID29 (ESRF), and X11 (EMBL Hamburg/DESY). For further details, see Table 1. Different single-wavelength data sets were collected using an ADSC Quantum-4 CCD detector at beamline BM14 (2W4K) or a MAR Mosaic 225-CCD detector at ID23-2 (2XUU and 4B4L), both at ESRF. Data were processed mainly within the CCP4 suite (Collaborative Computational Project, Number 4, 1994; Potterton et al., 2004). X-ray data were reduced using the programs MOSFLM (Leslie, 2006) and SCALA (Evans, 2006). Phases were determined by molecular replacement using the program PHASER (McCoy et al., 2007) using the structure of the DAPK1 catalytic domain (1JKL) as the search model. Model building and refinement was carried with COOT (Potterton et al., 2004) and REFMAC5 (Murshudov et al., 1997), respectively. Visible electron densities, used to identify the crystal structures in the study, comprise residues 2–302 (WT and E182A) and residues 5–303 (R302A). Coordinates and structure factors have been submitted to the PDB database with the accession codes 2W4K, 2XUU, and 4B4L. Complete statistics are shown in Table 1. The respective Ramachandran statistics indicating the fraction of residues in the favored/allowed/outlier regions of the Ramachandran diagram as defined by MOLPROBITY (Chen et al., 2010) are 98.3/1.7/0.0 (2W4K), 98.7/1.0/0.3 (2XUU), and 98.3/1.7/0.0 (4B4L). Figures were prepared using the Molecular Graphics System PyMOL (Schrödinger).

In Vitro Kinase Activity Assays

The kinetic activity of DAPK variants was analyzed using an in vitro kinase assay in which ATP consumption is coupled to the oxidation of NADH through pyruvate kinase and lactate dehydrogenase (Cook et al., 1982; Roskoski, 1983). Reactions were performed at 30°C in 100 μl reaction mixtures containing 2 U pyruvate kinase, 2 U lactate dehydrogenase, 2 mM phosphoenolpyruvate, 0.4 mM NADH, 0.5 mM $CaCl_2$, 10 mM KCl, 20 mM $MgCl_2$, and 0.2 mM DTT buffered in 60 mM HEPES (pH 7.2). The reaction mix, containing the ATP substrate, was incubated for 1 min at 30°C and initiated by the addition of the peptide substrate in a 2-fold dilution series. Saturating concentrations of ATP (2 mM) and peptide (500 μM) were determined empirically as

Substrate	-7	-6	-5	-4	-3	-2	-1	0	1	2	3	4	5	6	7	Position	PDB ID	Secondary Structure
DAPK1 (ARD)	A	R	K	K	W	K	Q	S	V	R	L	I	S	L	C	S308	2W4K, 2X0G	α-Helical (positions -7 to 7)
MLC-2	K	R	P	Q	R	A	T	S	N	V	F	A	M	F	D	S20	3TS5*	-
Beclin-1	L	S	R	R	L	K	V	T	G	D	L	F	D	I	M	T119	2P1L	α-Helical (positions -7 to 6)
P1-MCM3	K	T	I	E	R	R	Y	S	D	L	T	T	L	V	A	S160	n/a	
CAMKK 2	R	R	E	E	R	S	L	S	A	P	G	N	L	L	T	S511	n/a	
40S ribosomal protein S6	I	A	K	R	R	R	L	S	S	L	R	A	S	T	S	S235	n/a	
PPIase Pin1	H	S	Q	S	R	R	P	S	S	W	R	Q	E	K	I	S71	1PIN, 1F8A	-
Syntaxin-1A	I	I	M	D	S	S	I	S	K	Q	A	L	S	E	I	S188	3C98	α-Helical (positions 1 to 7)
Tropomyosin-1	H	A	L	N	D	M	T	S	I							S283	1C1G**	α-Helical (positions -7 to -2)

Figure 5. Sequence Representation of the Best-Described Human Substrates or Pseudosubstrates of DAPK1

The relative position to the phosphorylated residue (in green) as well as the respective position of the phosphorylated residue is indicated. Basic residues are colored in blue and acidic residues in red. If available, PDB IDs of the respective substrates are stated. In case a secondary structure is formed within the indicated sequence, this is highlighted. **Placopecten magellanicus* structure, 66% sequence identity to the indicated human sequence; ***Sus scrofa* structure, 100% sequence identity to the indicated human sequence; n/a, no structure available.

well as the rate-limiting kinase concentration (final concentration, 250 nM). Peptide substrate (KKRPQRRYSNVF) and variants (Velentza et al., 2001) were at least 90% pure (GenScript). Measurements were performed for 1 hr at 340 nm in a plate reader (TECAN, Infinite M1000), as described previously (Kiianitsa et al., 2003). Titrations were performed in duplicate with three independent repetitions using 500, 250, 125, 62.5, and 31.25 μM as peptide concentrations with saturating ATP concentrations. The reaction constants were calculated under pseudo-single-substrate conditions, in which one of the substrates was kept at saturating concentration. The reaction follows simple Michaelis-Menten kinetics, applied for calculation of the constants using a nonlinear least-squares best fit of the data with GraphPad Prism (version 5.00, GraphPad Software). For each experiment, at least three independent measurements were used (0–500 μM peptide substrate range). Kinetic experiments, in the presence of Ca^{2+}/CaM, were performed by mixing purified DAPK1 and Ca^{2+}/CaM (at 10-fold molar excess) to take into account possible secondary effects such as potential differences in CaM binding and Ser308 autophosphorylation by different DAPK1 variants. We compared this setup with a previously established coexpression and purification protocol (de Diego et al., 2010), which maximizes enrichment of DAKP1/CaM complexes. When DAPK1 and Ca^{2+}/CaM were mixed, WT DAPK1 reached an activity level of about half that of the coexpressed and purified DAPK1/CaM complex (Table S1). This ratio was confirmed for the DAPK1 (R302A) mutant; hence, Arg302 removal does not induce major secondary effects.

To further assess the proteins properties for the kinase activity assay, we analyzed S308 autophosphorylation levels. A total of 10 μg of the respective purified recombinant DAPK1 was treated for 30 min with 5 mM Mg^{2+} and 1 mM ATP to correct for purification variations. Samples were separated by SDS-PAGE and analyzed by western blot using an anti-DAPK1 phosphoS308 antibody (D4941, Sigma-Aldrich). Bands were visualized using a horseradish-peroxidase-tagged secondary anti-mouse antibody. The analysis was performed in triplicate and a representative blot is shown (Figure S4A). In addition, the CaM binding capacity of DAPK1 variants was analyzed by pull-down. CaM Sepharose (17-0529-01 GE Healthcare Life Sciences) was incubated with 100 μg of the respective purified DAPK1 in the presence of 5mM Ca^{2+} for 1 hr. The supernatant was collected and analyzed by SDS-PAGE together with the beads, which were washed extensively before analysis. The analysis was performed in triplicate and a representative gel image is shown (Figure S4B).

Cellular Blebbing Assays

Cellular activity of DAPK1 through MLC-2 phosphorylation was determined with a plasma membrane blebbing assay (Bialik et al., 2004; Bovellan et al., 2010). Human embryonic kidney 293T (HEK293T) cells were transfected with Fugene (Promega) or lipofectamine 2000 (Invitrogen) according to the manufacturer's instructions. For microscopy experiments, cells were plated out 24 hr before transfection on glass bottom dishes (MatTek) and live cells were imaged 24 or 48 hr posttransfection with a 25× or a 63× objective on an UltraVIEW VoX (Perkin Elmer) confocal microscope or on an AxioObserver Z1 (Carl Zeiss MicroImaging) inverted fluorescence microscope. Where indicated, cells were treated with 2.5 μM TG for 15 min before imaging. Images were processed with ImageJ; cells were scored manually into either a blebbing or normal phenotype. For each replicate, the percentage of blebbing cells for DAPK1 WT was normalized to 1 to exclude environmental effects, resulting in a relative blebbing ratio as compared to WT. The percentage of blebbing cells on the total imaged cells is also depicted in Figure 3. Equal kinase expression was confirmed by fluorescence intensity in microscopy and control flow cytometric analysis (MoFlo cell sorter, Beckman Coulter). FITC Annexin V (BD Biosciences) and propidium iodide staining in flow cytometry were used to determine the vitality of the cells as described (van Engeland et al., 1998). This control analysis did not show significant differences in apoptosis or necrosis for the DAPK1 variants used compared to control enhanced cyan fluorescent protein (ECFP)-transfected cells.

Sequence Alignments

Protein phosphorylation targets of DAPK1 and the corresponding sequences were retrieved from the Phospho.ELM database (Dinkel et al., 2011) and supplemented with literature data (Lin et al., 2010). Sequences near known phosphorylation sites were manually aligned and visualized with Jalview (Waterhouse et al., 2009). The kinase domain sequences of human CAMK and DAPK-related kinases were retrieved from UniProt (http://www.uniprot.org/), aligned with ClustalW; Thompson et al., 1994) within Jalview, by selecting at least one representative member from each branch of the CAMK family (Manning et al., 2002). For the grouping of PEF/Y motif-containing kinases listed in Table 2, all 518 human kinase domains listed in the KinBase database (http://kinase.com/kinbase) were aligned and examined for the presence of the motif. Likewise, a CAMK phylogenetic tree was acquired from the same database and node age calculation and visualization were done with FigTree (v1.4.0; http://tree.bio.ed.ac.uk/software/figtree).

Model Generation of an Extended DAPK1 Version, Including a Ser308 Autophosphorylation Site

The purpose of modeling an extended DAPK1 fragment was to confirm intramolecular phosphorylation of Ser308 as a plausible mechanism, thus allowing structural details of the ARD—to the extent that they are visible in experimental structures—to be considered as a pseudosubstrate. We used a previously determined structure of phosphorylase kinase, which shares 28% sequence identity with DAPK1, in complex with a seven-residue substrate peptide (Protein Data Bank [PDB] code 2PHK), as a template. The peptide in this structure (RQMSFRL) matches most residues 305–311 (WKQSVRL) that are missing in our DAPK1 structure (PDB code 2W4K), taking the phosphorylation site as a reference. Upon superposition of 2PHK and 2W4K, initially we removed the first two residues of the peptide to allow annealing with the C-terminal residue Arg302 in 2W4K and mutated those residue positions that differ in 2PHK and 2W4K (Gln307 and Val309). Subsequently, a preliminary model was built by inserting four residues (KKWK, residues 303–306) and refined with FlexPepDock (Raveh et al., 2010). The ten most highly scoring models were optimized via molecular dynamics simulation software (NAMD version 2.7b4; Phillips et al., 2005) with Amber force field. After optimization, the model with the lowest energy was selected as the final DAPK1 (2-311) model. An alternative model (not displayed) was also generated with the same approach starting from the structure of CaMKII (PDB ID 3KK8). Both models produced the same overall conformation with minor differences in side-chain orientation. The coordinates of the phosphorylase kinase-based model are available in 3D Molecular Model S1.

ACCESSION NUMBERS

Coordinates and structure factors have been submitted to the PDB database with the accession codes 2W4K, 2XUU, and 4B4L.

SUPPLEMENTAL INFORMATION

Supplemental Information includes Supplemental Experimental Procedures, four figures, one table, and one 3D molecular structure and can be found with this article online at http://dx.doi.org/10.1016/j.chembiol.2013.12.008.

ACKNOWLEDGMENTS

This work was supported by European Commission grants CAMKIN (HPRN-CT-2002- 00252) and SPINE2-COMPLEXES (LSHG-CT-2006-031220). I.d.D. was supported by a grant from the Spanish Ministry of Science and Innovation MICINN (ES-2006-0149). K.T. and X.L. were supported by an EMBL Interdisciplinary Postdoc (EIPOD) fellowship under Marie Curie Actions (COFUND). This study was technically supported by the EMBL Advanced Light Microscopy Facility, the EMBL Flow Cytometry Core Facility, and the High Throughput Crystallization Laboratory Facility at EMBL Hamburg. We thank Janet Thornton, Maja Köhn, Toby Gibson, and Carsten Schulz for the computational resource support and kind suggestions.

Received: June 10, 2013
Revised: December 6, 2013
Accepted: December 8, 2013
Published: January 16, 2014

REFERENCES

Alexander, J., Lim, D., Joughin, B.A., Hegemann, B., Hutchins, J.R., Ehrenberger, T., Ivins, F., Sessa, F., Hudecz, O., Nigg, E.A., et al. (2011). Spatial exclusivity combined with positive and negative selection of phosphorylation motifs is the basis for context-dependent mitotic signaling. Sci. Signal. *4*, ra42.

Barretina, J., Caponigro, G., Stransky, N., Venkatesan, K., Margolin, A.A., Kim, S., Wilson, C.J., Lehár, J., Kryukov, G.V., Sonkin, D., et al. (2012). The Cancer Cell Line Encyclopedia enables predictive modelling of anticancer drug sensitivity. Nature *483*, 603–607.

Ben-Shimon, A., and Niv, M.Y. (2011). Deciphering the Arginine-binding preferences at the substrate-binding groove of Ser/Thr kinases by computational surface mapping. PLoS Comput. Biol. *7*, e1002288.

Bialik, S., and Kimchi, A. (2012). Biochemical and functional characterization of the ROC domain of DAPK establishes a new paradigm of GTP regulation in ROCO proteins. Biochem. Soc. Trans. *40*, 1052–1057.

Bialik, S., Bresnick, A.R., and Kimchi, A. (2004). DAP-kinase-mediated morphological changes are localization dependent and involve myosin-II phosphorylation. Cell Death Differ. *11*, 631–644.

Bialik, S., Berissi, H., and Kimchi, A. (2008). A high throughput proteomics screen identifies novel substrates of death-associated protein kinase. Mol. Cell. Proteomics *7*, 1089–1098.

Bovellan, M., Fritzsche, M., Stevens, C., and Charras, G. (2010). Death-associated protein kinase (DAPK) and signal transduction: blebbing in programmed cell death. FEBS J. *277*, 58–65.

Chao, L.H., Pellicena, P., Deindl, S., Barclay, L.A., Schulman, H., and Kuriyan, J. (2010). Intersubunit capture of regulatory segments is a component of cooperative CaMKII activation. Nat. Struct. Mol. Biol. *17*, 264–272.

Chen, V.B., Arendall, W.B., 3rd, Headd, J.J., Keedy, D.A., Immormino, R.M., Kapral, G.J., Murray, L.W., Richardson, J.S., and Richardson, D.C. (2010). MolProbity: all-atom structure validation for macromolecular crystallography. Acta Crystallogr. D Biol. Crystallogr. *66*, 12–21.

Cook, P.F., Neville, M.E., Jr., Vrana, K.E., Hartl, F.T., and Roskoski, R., Jr. (1982). Adenosine cyclic 3′,5′-monophosphate dependent protein kinase: kinetic mechanism for the bovine skeletal muscle catalytic subunit. Biochemistry *21*, 5794–5799.

Collaborative Computational Project, Number 4 (1994). The CCP4 suite: programs for protein crystallography. Acta Crystallogr. D Biol. Crystallogr. *50*, 760–763.

de Diego, I., Kuper, J., Bakalova, N., Kursula, P., and Wilmanns, M. (2010). Molecular basis of the death-associated protein kinase-calcium/calmodulin regulator complex. Sci. Signal. *3*, ra6.

Dinkel, H., Chica, C., Via, A., Gould, C.M., Jensen, L.J., Gibson, T.J., and Diella, F. (2011). Phospho.ELM: a database of phosphorylation sites—update 2011. Nucleic Acids Res. *39* (Database issue), D261–D267.

Ellis, J.J., and Kobe, B. (2011). Predicting protein kinase specificity: Predikin update and performance in the DREAM4 challenge. PLoS ONE *6*, e21169.

Evans, P. (2006). Scaling and assessment of data quality. Acta Crystallogr. D Biol. Crystallogr. *62*, 72–82.

Fujii, K., Zhu, G., Liu, Y., Hallam, J., Chen, L., Herrero, J., and Shaw, S. (2004). Kinase peptide specificity: improved determination and relevance to protein phosphorylation. Proc. Natl. Acad. Sci. USA *101*, 13744–13749.

Fujita, Y., and Yamashita, T. (2013). Role of DAPK in neuronal cell death. Apoptosis. Published online October 10, 2013. http://dx.doi.org/10.1007/s10495-013-0917-4.

Goldsmith, E.J., Akella, R., Min, X., Zhou, T., and Humphreys, J.M. (2007). Substrate and docking interactions in serine/threonine protein kinases. Chem. Rev. *107*, 5065–5081.

Graves, P.R., Winkfield, K.M., and Haystead, T.A. (2005). Regulation of zipper-interacting protein kinase activity in vitro and in vivo by multisite phosphorylation. J. Biol. Chem. *280*, 9363–9374.

Greenman, C., Stephens, P., Smith, R., Dalgliesh, G.L., Hunter, C., Bignell, G., Davies, H., Teague, J., Butler, A., Stevens, C., et al. (2007). Patterns of somatic mutation in human cancer genomes. Nature *446*, 153–158.

Hornbeck, P.V., Kornhauser, J.M., Tkachev, S., Zhang, B., Skrzypek, E., Murray, B., Latham, V., and Sullivan, M. (2012). PhosphoSitePlus: a comprehensive resource for investigating the structure and function of experimentally determined post-translational modifications in man and mouse. Nucleic Acids Res. *40* (Database issue), D261–D270.

Kawai, T., Matsumoto, M., Takeda, K., Sanjo, H., and Akira, S. (1998). ZIP kinase, a novel serine/threonine kinase which mediates apoptosis. Mol. Cell. Biol. *18*, 1642–1651.

Kemp, B.E., and Pearson, R.B. (1985). Spatial requirements for location of basic residues in peptide substrates for smooth muscle myosin light chain kinase. J. Biol. Chem. *260*, 3355–3359.

Kemp, B.E., Pearson, R.B., and House, C. (1983). Role of basic residues in the phosphorylation of synthetic peptides by myosin light chain kinase. Proc. Natl. Acad. Sci. USA *80*, 7471–7475.

Kemp, B.E., Parker, M.W., Hu, S., Tiganis, T., and House, C. (1994). Substrate and pseudosubstrate interactions with protein kinases: determinants of specificity. Trends Biochem. Sci. *19*, 440–444.

Kiianitsa, K., Solinger, J.A., and Heyer, W.D. (2003). NADH-coupled microplate photometric assay for kinetic studies of ATP-hydrolyzing enzymes with low and high specific activities. Anal. Biochem. *321*, 266–271.

Kornev, A.P., and Taylor, S.S. (2010). Defining the conserved internal architecture of a protein kinase. Biochim. Biophys. Acta *1804*, 440–444.

Leslie, A.G. (2006). The integration of macromolecular diffraction data. Acta Crystallogr. D Biol. Crystallogr. *62*, 48–57.

Lin, Y., Hupp, T.R., and Stevens, C. (2010). Death-associated protein kinase (DAPK) and signal transduction: additional roles beyond cell death. FEBS J. *277*, 48–57.

Lowe, E.D., Noble, M.E., Skamnaki, V.T., Oikonomakos, N.G., Owen, D.J., and Johnson, L.N. (1997). The crystal structure of a phosphorylase kinase peptide substrate complex: kinase substrate recognition. EMBO J. *16*, 6646–6658.

Manning, G., Whyte, D.B., Martinez, R., Hunter, T., and Sudarsanam, S. (2002). The protein kinase complement of the human genome. Science *298*, 1912–1934.

 ©2014 Elsevier Ltd All rights reserved

Mayans, O., van der Ven, P.F., Wilm, M., Mues, A., Young, P., Fürst, D.O., Wilmanns, M., and Gautel, M. (1998). Structural basis for activation of the titin kinase domain during myofibrillogenesis. Nature *395*, 863–869.

Mayans, O., Benian, G.M., Simkovic, F., and Rigden, D.J. (2013). Mechanistic and functional diversity in the mechanosensory kinases of the titin-like family. Biochem. Soc. Trans. *41*, 1066–1071.

McCoy, A.J., Grosse-Kunstleve, R.W., Adams, P.D., Winn, M.D., Storoni, L.C., and Read, R.J. (2007). Phaser crystallographic software. J. Appl. Cryst. *40*, 658–674.

Moore, M.J., Adams, J.A., and Taylor, S.S. (2003). Structural basis for peptide binding in protein kinase A. Role of glutamic acid 203 and tyrosine 204 in the peptide-positioning loop. J. Biol. Chem. *278*, 10613–10618.

Murshudov, G.N., Vagin, A.A., and Dodson, E.J. (1997). Refinement of macromolecular structures by the maximum-likelihood method. Acta Crystallogr. D Biol. Crystallogr. *53*, 240–255.

Obenauer, J.C., Cantley, L.C., and Yaffe, M.B. (2003). Scansite 2.0: Proteome-wide prediction of cell signaling interactions using short sequence motifs. Nucleic Acids Res. *31*, 3635–3641.

Pellicena, P., and Kuriyan, J. (2006). Protein-protein interactions in the allosteric regulation of protein kinases. Curr. Opin. Struct. Biol. *16*, 702–709.

Phillips, J.C., Braun, R., Wang, W., Gumbart, J., Tajkhorshid, E., Villa, E., Chipot, C., Skeel, R.D., Kalé, L., and Schulten, K. (2005). Scalable molecular dynamics with NAMD. J. Comput. Chem. *26*, 1781–1802.

Pike, A.C., Rellos, P., Niesen, F.H., Turnbull, A., Oliver, A.W., Parker, S.A., Turk, B.E., Pearl, L.H., and Knapp, S. (2008). Activation segment dimerization: a mechanism for kinase autophosphorylation of non-consensus sites. EMBO J. *27*, 704–714.

Potterton, L., McNicholas, S., Krissinel, E., Gruber, J., Cowtan, K., Emsley, P., Murshudov, G.N., Cohen, S., Perrakis, A., and Noble, M. (2004). Developments in the CCP4 molecular-graphics project. Acta Crystallogr. D Biol. Crystallogr. *60*, 2288–2294.

Raval, A., Tanner, S.M., Byrd, J.C., Angerman, E.B., Perko, J.D., Chen, S.S., Hackanson, B., Grever, M.R., Lucas, D.M., Matkovic, J.J., et al. (2007). Downregulation of death-associated protein kinase 1 (DAPK1) in chronic lymphocytic leukemia. Cell *129*, 879–890.

Raveh, B., London, N., and Schueler-Furman, O. (2010). Sub-angstrom modeling of complexes between flexible peptides and globular proteins. Proteins *78*, 2029–2040.

Roskoski, R., Jr. (1983). Assays of protein kinase. Methods Enzymol. *99*, 3–6.

Schumacher, A.M., Velentza, A.V., and Watterson, D.M. (2002). Death-associated protein kinase as a potential therapeutic target. Expert Opin. Ther. Targets *6*, 497–506.

Scott, J.W., Norman, D.G., Hawley, S.A., Kontogiannis, L., and Hardie, D.G. (2002). Protein kinase substrate recognition studied using the recombinant catalytic domain of AMP-activated protein kinase and a model substrate. J. Mol. Biol. *317*, 309–323.

Shohat, G., Spivak-Kroizman, T., Cohen, O., Bialik, S., Shani, G., Berrisi, H., Eisenstein, M., and Kimchi, A. (2001). The pro-apoptotic function of death-associated protein kinase is controlled by a unique inhibitory autophosphorylation-based mechanism. J. Biol. Chem. *276*, 47460–47467.

Steichen, J.M., Iyer, G.H., Li, S., Saldanha, S.A., Deal, M.S., Woods, V.L., Jr., and Taylor, S.S. (2010). Global consequences of activation loop phosphorylation on protein kinase A. J. Biol. Chem. *285*, 3825–3832.

Temmerman, K., Simon, B., and Wilmanns, M. (2013). Structural and functional diversity in the activity and regulation of DAPK-related protein kinases. FEBS J. *280*, 5533–5550.

Thompson, J.D., Higgins, D.G., and Gibson, T.J. (1994). CLUSTAL W: improving the sensitivity of progressive multiple sequence alignment through sequence weighting, position-specific gap penalties and weight matrix choice. Nucleic Acids Res. *22*, 4673–4680.

Ubersax, J.A., and Ferrell, J.E., Jr. (2007). Mechanisms of specificity in protein phosphorylation. Nat. Rev. Mol. Cell Biol. *8*, 530–541.

van Engeland, M., Nieland, L.J., Ramaekers, F.C., Schutte, B., and Reutelingsperger, C.P. (1998). Annexin V-affinity assay: a review on an apoptosis detection system based on phosphatidylserine exposure. Cytometry *31*, 1–9.

Velentza, A.V., Schumacher, A.M., Weiss, C., Egli, M., and Watterson, D.M. (2001). A protein kinase associated with apoptosis and tumor suppression: structure, activity, and discovery of peptide substrates. J. Biol. Chem. *276*, 38956–38965.

Waterhouse, A.M., Procter, J.B., Martin, D.M., Clamp, M., and Barton, G.J. (2009). Jalview Version 2—a multiple sequence alignment editor and analysis workbench. Bioinformatics *25*, 1189–1191.

Wang, L., Hauser, E.R., Shah, S.H., Pericak-Vance, M.A., Haynes, C., Crosslin, D., Harris, M., Nelson, S., Hale, A.B., Granger, C.B., et al. (2007). Peakwide mapping on chromosome 3q13 identifies the kalirin gene as a novel candidate gene for coronary artery disease. Am. J. Hum. Genet. *80*, 650–663.

Yaffe, M.B., Leparc, G.G., Lai, J., Obata, T., Volinia, S., and Cantley, L.C. (2001). A motif-based profile scanning approach for genome-wide prediction of signaling pathways. Nat. Biotechnol. *19*, 348–353.

Yang, J., Cron, P., Good, V.M., Thompson, V., Hemmings, B.A., and Barford, D. (2002). Crystal structure of an activated Akt/protein kinase B ternary complex with GSK3-peptide and AMP-PNP. Nat. Struct. Biol. *9*, 940–944.

Zhu, G., Fujii, K., Liu, Y., Codrea, V., Herrero, J., and Shaw, S. (2005). A single pair of acidic residues in the kinase major groove mediates strong substrate preference for P-2 or P-5 arginine in the AGC, CAMK, and STE kinase families. J. Biol. Chem. *280*, 36372–36379.